Integrated Use of Time-Frequency Wavelet Decompositions for Fault Location in Distribution Networks: Theory and Experimental Validation

A. Borghetti, M. Bosetti, M. Paolone and A. Abur

Abstract –**The paper presents a procedure for fault location in distribution networks. The proposed procedure is based on the analysis of electromagnetic transients associated with fault-originated travelling waves. The analysis is carried out by means of the integrated time-frequency wavelet decomposition that improves the identification accuracy of specific frequencies associated with the faulted branch and the fault location.**

In order to validate the proposed procedure, the voltage measurements obtained during several fault tests in a reduced scale setup reproducing a distribution network feeder are used. The paper illustrates the performance of the proposed procedure when applied to the recorded fault transients in a real distribution network.

Keywords: Fault location, electromagnetic transients, distribution networks, continuous wavelet transform, power quality.

I. Introduction

THE accurate fault location in medium voltage distribution networks is one of the aspects that has a major impact on the service continuity. Moreover, switching transients associated to both fault location searching techniques and subsequent service restoration reconfiguration maneuvers may also affect power quality of the distribution networks [1].

Various procedures for fault location assessment are described in the literature [2]. Some procedures analyze pre and post-fault voltage and currents by referring to their steady state values [3-5], whilst others are based on the analysis of fault-originated electromagnetic transients, (i.e. traveling waves generated by the fault itself [6-10].

The procedure presented in this paper belongs to the second of the above mentioned categories and combines the method presented in [8,9] with the one of [11,12]. As in [11,12], the procedure proposed in this paper is based on the wavelet analysis of fault-originated electromagnetic transients by applying the continuous wavelet transformation (CWT). The CWT analysis is performed by making use of specific mother wavelets inferred from the voltage transient waveforms [12]. Such an analysis is aimed at identifying characteristic frequencies associated to the faulted branch and to the fault location. Whilst in [11,12] the characteristic frequencies are estimated by means of a CWT analysis of the transient waveforms only in frequency domain, the procedure presented in this paper extends such an analysis to both time and frequency CWT decompositions [8,9]. This improves the fault location accuracy with respect to the method proposed in [11,12].

The paper describes the theory of the proposed fault location procedure. In order to illustrate the characteristics of the proposed approach, we refer to the fault transient waveforms obtained during several experimental fault tests in a specifically developed reduced scale setup of a distribution network feeder. The paper finally illustrates also the application of the proposed procedure to the fault transients recorded during a fault event in a real distribution network.

The structure of the paper is the following: Section II illustrates the reduced-scale experimental setup that represents a distribution network feeder; Section III illustrates the theory of the proposed procedure with reference to the voltage transients recorded during some fault tests in the reduced scale setup of section II; Section IV illustrates the validation of the procedure with reference to several faults events emulated in the reduced scale setup and for the case a fault event occurred in a real distribution network. Section V concludes the paper.

II. Reduced-scale experimental setup

The simulation of fault transients is typically performer by means of electromagnetic transient programs that allows to represent the propagation phenomena that takes place in the line feeders (e.g. [13,14]). Such a kind of simulation is able to accurately reproduce electromagnetic fault transients and in the previous paper [8,9,11,12] has been successfully used.

In order to extend the application of the proposed fault location algorithm also to real electromagnetic fault transients, in this paper they are experimentally obtained by means of a reduced-scale experimental setup aimed at reproducing the response of single-phase cable feeders.

The two topologies shown in Fig. 1 have been considered (a single feeder and a feeder including a lateral branch).

The assumed scale factor is of 1:50. All cable lengths are divided by this factor whilst the frequency of the reduced scale power supply is multiplied by such a factor in order to keep the ratio of the feeding voltage wavelength to the cable

A. Borghetti, M. Bosetti and M. Paolone are with the Department of Electrical Engineering, University of Bologna, Bologna, Italy (e-mail: {alberto.borghetti; mauro.bosetti; mario.paolone}@unibo.it).

A. Abur is with the Electrical and Computer Engineering Department of the Northeastern University, Boston, Massachusetts, USA (e-mail: abur@ece.neu.edu).

Paper submitted to the International Conference on Power Systems Transients (IPST2009) in Kyoto, Japan June 3-6, 2009

lengths constant. The reduced scale cable lengths are reported in Fig. 1 and the equivalent power supply frequency, for a real scale frequency of 50 Hz, is equal to 2.5 kHz.

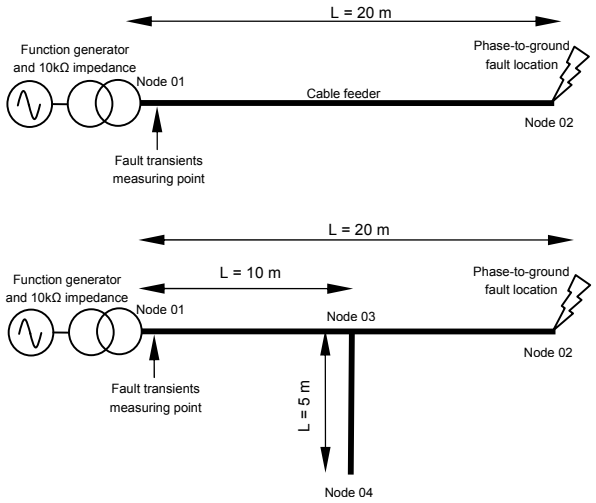

Fig. 1. Topologies of the reduced scale setup aimed at reproducing electromagnetic fault transients: a) single feeder, b) feeder including a lateral branch.

A standard RG58 signal cable with a 50 Ω surge impedance and a measured propagation speed of $1.786 \cdot 10^8$ m/s is adopted for the network lines.

The feeding voltage is provided by an Agilent 33120A function generator placed in series with a 10 kΩ impedance in order to represent, as a first approximation, the primary substation transformer response to the fault-generated travelling waves.

The fault between the cable shield and its inner conductor is generated by means of a fast TTL micro-switch triggered by a National Instruments 9401 high-speed digital I/O board.

The fault-originated waveforms are recorded at the junction between the cable feeder and the 2 kΩ lumped impedance. The signals are captured by a LeCroy LT264 8-bit 1-GSa/s digital oscilloscope.

III. Integrated Use of Time-Frequency Wavelet Decomposition Applied to Fault Transients

As in [11,12], the fault location procedure is based on the identification of the characteristic frequencies associated with the specific paths followed by the fault-originated traveling waves.

Assuming the network topology and the traveling wave speed v_i of the *i-th* propagation mode [15,16] are known, frequency $f_{p,i}$ of mode *i* through path *p* can be evaluated as

$$f_{p,i} = \frac{v_i}{n_p L_p} \tag{1}$$

where L_p is the length of the *p-th* path and $n_p (\in \mathbf{N})$ is the number of times a given travelling wave propagates along path *p* before attaining its original polarity. *p*-1 values are used to identify the faulted section and the remaining one is used to identify the distance between observation point *m* and the fault location.

Coefficient n_p depends on the sign of the reflection coefficients of the two ends of the travelled path. This implies that n_p is equal to 2 or 4 if the sign of the reflection coefficients is the same or different respectively. In particular, terminals where a power transformer is connected can be considered as open circuits with a n_p close to +1, whereas terminals that appear as junctions between more than two lines will have a negative n_p. Furthermore, the fault point can be assumed to have a n_p close to -1.

Fig. 2 shows the fault-originated transients corresponding to the two topologies of Fig. 1. The fault triggered by the TTL micro-switch can be assumed as a step-function source. The voltage transients of Fig. 2 can be seen as the result of the superposition of different square waves each one having a fundamental frequency given by (1). This behavior is particularly clear for the case of Fig. 2a which corresponds to the single cable feeder.

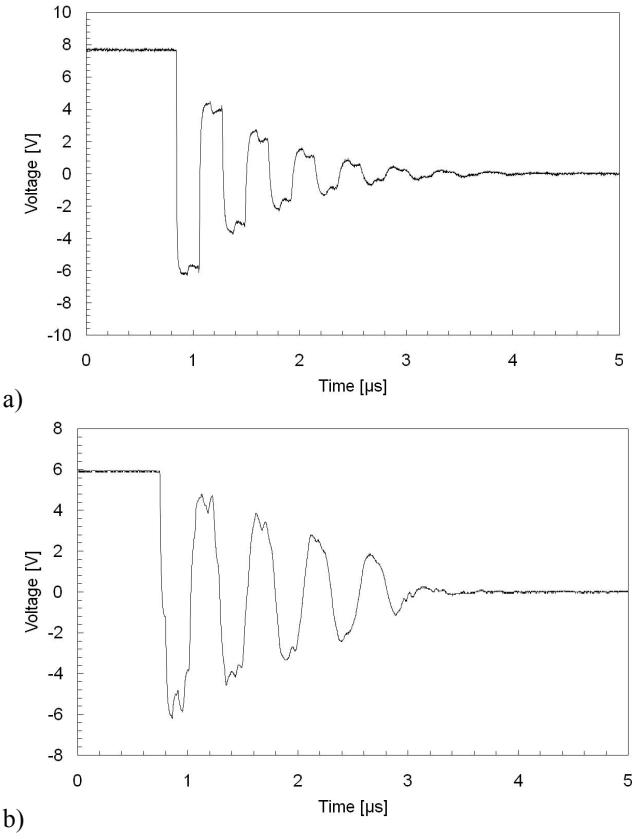

Fig. 2. Reduced scale voltage transients in correspondence of the measurement point of Fig. 1: a) configuration of Fig. 1a, b) configuration of Fig. 1b.

Table I shows the theoretical frequencies observed at Node 01 of Fig. 1 obtained by applying (1) to the two considered network configurations.

TABLE I. CHARACTERISTIC FREQUENCIES RELEVANT TO THE PROPAGATION PATHS OF TOPOLOGIES REPORTED IN FIG. 1 (REDUCED SCALE CABLE LENGTH).

Single feeder		
Path	Path length $n_p \cdot L_p$ (m)	Theoretical frequencies $f_{p,i}$ (traveling speed equal to $1.786 \cdot 10^8$ m/s) (MHz)
Node 01-02	4x20 (n_p=4)	2.233
Feeder including a lateral branch		
Node 01-02	4x20 (n_p=4)	2.233
Node 01-03	4x10 (n_p=4)	4.465
Node 01-04	2x15 (n_p=2)	5.953

Concerning the identification of the characteristic frequencies, it is worth noting that the fault transient is characterized by a continuous spectrum due to its time-variant properties. Therefore these frequencies are identified by means of the continuous wavelet transform (CWT) that allows a good frequency resolution at low frequencies and a good time resolution at high frequencies [17]. These characteristics allow the identification of high frequency components very close in time and low frequency components very close in frequency.

In order to overcome some limitations relevant to the use of traditional mother wavelets (e.g. the Morlet one) in this paper the CWT analysis has been performed by using fault-inferred mother wavelets using the approach proposed in [12].

The numerical implementation of the CWT applied to signal $s(t)$ is well known and given by

$$C(a,b) = C(a, iT_s) = T_S \frac{1}{\sqrt{|a|}} \sum_{n=0}^{N-1} \psi^* \left[\frac{(n-i)T_S}{a} \right] s(nT_S) \quad (2)$$

where:

- $C(a,b)$ is the result of the CWT and represents a bi-dimensional function of time and frequency. In particular, coefficients $C(a,b)$ can be seen as similarity indices between the signal and the so-called daughter wavelet located at position b with scale a[1];
- T_s is the sampling time (in our reduced scale setup it is equal to 10^{-9} s);

The sum of the squared values of all coefficients belonging to the same scale, which are denoted as CWT signal energy $E_{CWT}(a)$, identifies a "scalogram" which provides the weight of each frequency component [18]:

$$E_{cwt}(a) = \sum_{n=0}^{N-1} \left(C(a, nT_s) \right)^2 \quad (3)$$

In the approach proposed in [11,12], the identification of the characteristic frequencies $f_{p,i}$ associated to the fault location was realized by inspecting the relative maximum peaks of the obtained scalogram $E_{cwt}(a)$. Such an approach disregards the information provided by the CWT time decomposition that can also be used to successfully locate the fault as proposed in [8,9].

The improvement introduced by the proposed method is due to the integrated time-frequency analysis which involves a two-step identification of the characteristic frequencies. The first step consists of an initial estimation of such frequencies $f_{p,i}^*$ as done in [11,12]. The second step improves the initial estimate by identifying the time differences between local maximum of the signal coefficients $C(a,b)$ defined by (2) in the frequency range centered at the previously identified frequency $f_{p,i}^*$.

Consider the configuration shown in Fig. 1a (single cable feeder) as a simple example to illustrate the use of the improved procedure. As shown in Table I, this configuration has a single characteristic frequency $f_{p,i}$ equal to 2.233 MHz. Fig. 3 shows the obtained scalogram relevant to the signal energy values $E_{cwt}(a)$ provided by (3) by using the procedure described [11,12] and a frequency $f_{p,i}^*$ of 2.162 MHz is identified. The error between the identified and theoretical frequency of Table I is of 3.2 % which corresponds to a fault location error of 3.3 %.

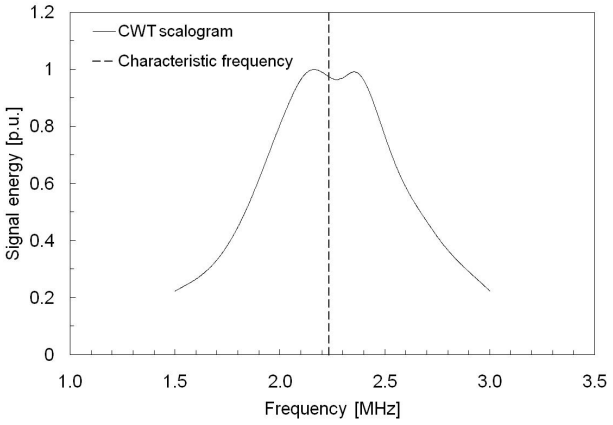

Fig. 3. Energy scalogram relevant to the CWT analysis of the fault transient of Fig. 2a relevant to the single cable configuration of Fig. 1a.

As illustrated above, the $f_{p,i}^*$ of 2.162 MHz is then used to explore time differences between local maximum in the signal coefficients $C(a,b)$. In particular, Fig. 4 shows the local maximum of $C(a,b)$ that allows to identify a time difference of 0.4425 μs that corresponds to an identified characteristic frequency of 2.26 MHz. This yields a frequency error of 1.2 % and a fault location error of 1.2 %. It is important to note that the identified time difference between peak values remains constant in the considered frequency range.

As evident from the above results an important error reduction in estimating the fault location can be achieved. In the following section the application of the improved fault location procedure is presented for the reduced scale configuration of Fig. 1b and for a real distribution network configuration.

[1] Parameter a corresponds to the scale factor and product $i \cdot T_s$ corresponds to the so-called time shifting factor b. It is worth nothing that if the center frequency of the mother wavelet $\psi(t)$ is F_0, the one of the daughter-wavelet $\psi(at)$ is F_0/a.

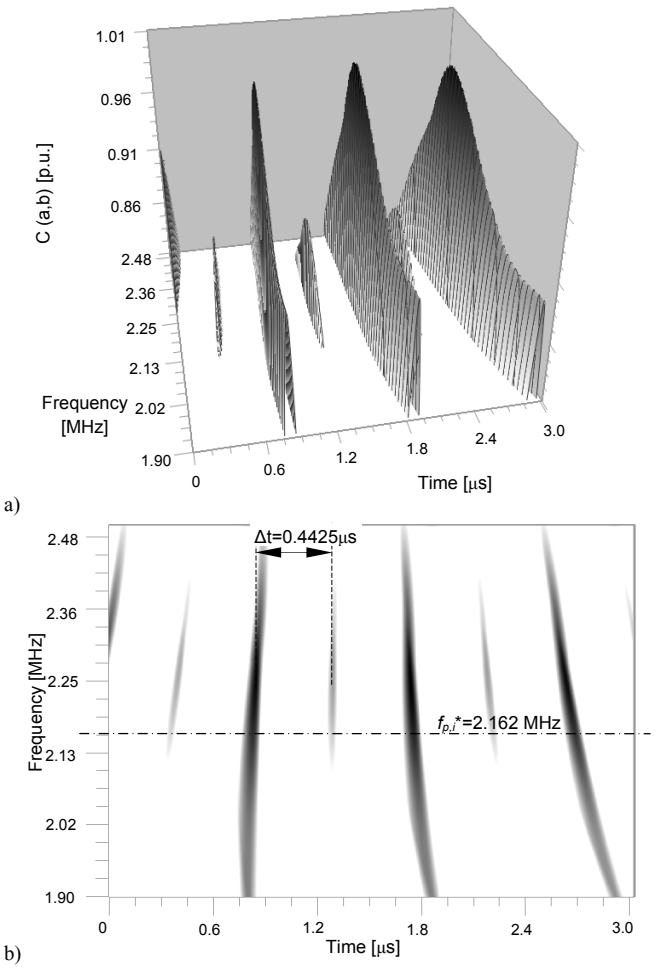

Fig. 4. Coefficients $C(a,b)$ obtained by means of the CWT analysis applied to the fault transient of Fig. 2a: improved estimation of the estimation of the characteristic frequency associated to the faulted path between nodes 01-02.

IV. Experimental validation

This section of the paper contains further experimental validation of the proposed fault location procedure by making reference to more complex network topologies. In particular, two case studies are presented: the first one refers to the configuration of Fig. 1b and the second one to a set of fault transients recorded in a real distribution network.

A. Reduced scale experimental setup: feeder including a lateral branch

Consider the reduced scale network topology shown in Fig. 1b and to the fault transients illustrated in Fig. 2b. Table I gives the three characteristic frequencies associated with the fault occuring at the end of the main feeder.

Fig. 5 shows the scalogram of the signal energy values $E_{cwt}(a)$ of (3) obtained by using the procedure described [11,12]. The identified frequencies are shown in Table II. These results imply that the error in the identified characteristic frequency for the given fault location is equal to 11.3 % and the fault location error is equal to 12.7 %.

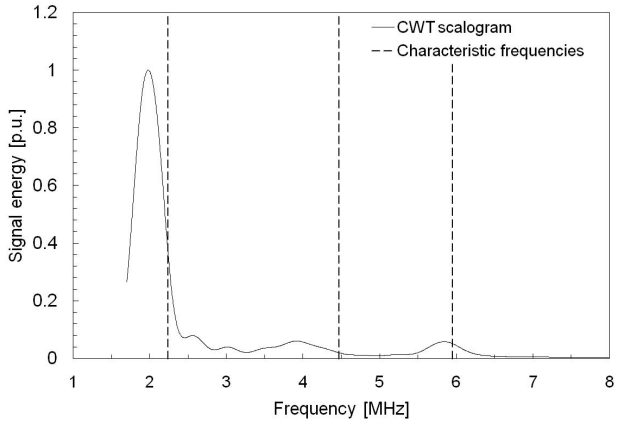

Fig. 5. Energy scalogram relevant to the CWT analysis of the fault transient of Fig. 2b relevant to the single cable configuration of Fig. 1b.

TABLE II. Characteristic and CWT identified frequencies using the approach of [11,12] relevant to the propagation paths of topologies reported in Fig. 1b (reduced scale cable length).

Path	Path length $n_p \cdot L_p$ (m)	Theoretical frequencies $f_{p,i}$ (traveling speed equal to $1.786 \cdot 10^8$ m/s) (MHz)	CWT identified frequencies $f_{p,i}$ by using the $E_{cwt}(a)$ (MHz)
Node 01-02	4x20 (n_p=4)	2.233	1.980
Node 01-03	4x10 (n_p=4)	4.465	3.922
Node 01-04	2x15 (n_p=2)	5.953	5.844

Similar to the case of the single cable feeder, Fig. 6 shows the analysis relevant to the identification of time differences between local maximum of the coefficients $C(a,b)$ in the frequency range centered in the CWT identified frequency $f_{p,i}$ by using the $E_{cwt}(a)$.

Fig. 6 shows the results obtained for the characteristic frequency of the fault location path between node 01 and node 02, where a time difference of 0.490 μs that corresponds to a characteristic frequency of 2.04 MHz is determined. This yields a frequency error of 8.6 % and a fault location error of 9.3 %. Hence, even in this more complex case the proposed approach yields an improvement estimate for the location of the fault.

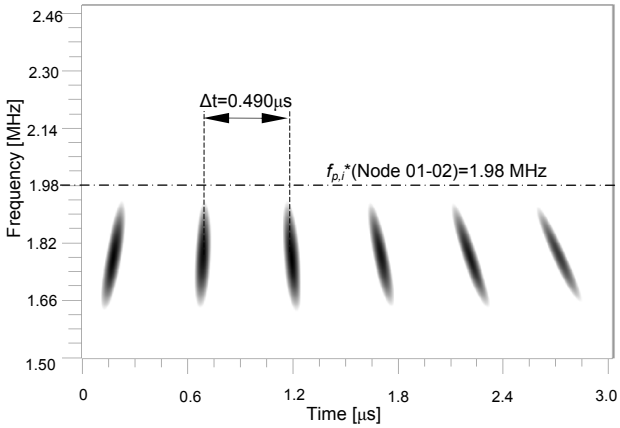

Fig. 6. Coefficients $C(a,b)$ obtained by means of the CWT analysis applied to the fault transient of Fig. 2b: improved estimation of the characteristic frequency associated with the faulted path between Nodes 01-02.

B. Fault transients recorded in a real distribution network

The proposed fault location procedure is also applied for location of a fault for which recorded electromagnetic transients were captured by means of the monitoring system illustrated in [19,20]. This monitoring system was suitably designed to measure lightning-originated transients and it was installed at some secondary sub-stations of a distribution network located in the northern region of Italy. It has the necessary sensor bandwidth and sampling frequency in order to accurately capture the electromagnetic transients originated by fault events [19].

The monitored distribution network is one of the 13 feeders that starts from the common primary 132/20 kV substation. The distribution network operates with isolated neutral grounding. The considered feeder is composed of three-phase overhead lines of overall length equal to 21.9 km, without any cables. The overhead lines consist of three conductors (without a shield wire), located at 10 m, 10.8 m and 10 m above ground, respectively. The feeder is composed of three branches, each 7-km long, arranged in a configuration shown in Fig. 7. The figure shows the network topology in plane coordinates using the Gauss-Boaga reference system.

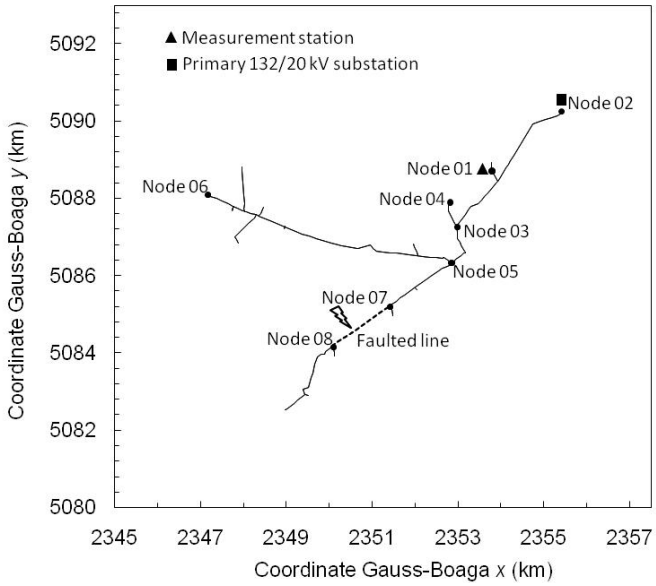

Fig. 7. Topology of the considered distribution network and point of interest.

The feeder is protected with one circuit breaker equipped with a three-level overcurrent relay (for multi-phase faults) and a three-level zero-sequence relay (for line-to ground-faults).

In the considered feeder, an additional monitoring system for protection manoeuvres is also installed at the primary substation [21]. It consists of PC-based recording system and receives signals from the different protection devices of the feeders connected to the substation, namely: overcurrent, 0-sequence and circuit-breaker operation relays. The system records any change of status relevant to each protection device in an ASCII file that can be post-processed. In addition to the protection change of status, the system provides the relevant UTC (Universal Time Code) value by means of a GPS unit characterized by a time uncertainty of 10 ms. Considering that the monitoring system that measures the electromagnetic transient is also equipped with a UTC-GPS unit, it is possible to associate each protection manoeuvre intervention to a specific recorded transient.

The system is in operation since 2007 and several fault events have been recorded. One of them, recorded on July 24, 2007 at 18h 25m 14s, has here used to validate the proposed procedure. The fault voltage transient, shown in Fig. 8, has been measured in correspondence of Node 01 of Fig. 7.

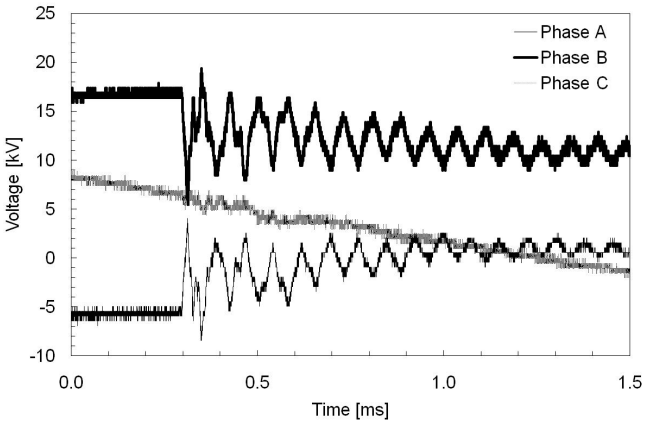

Fig. 8. Voltage transient observed in correspondence of Node 01 due to a fault between Nodes 07-08 of Fig. 7.

The location of this fault was identified by the distribution network maintenance crew as the dotted 'faulted line' reported in Fig. 7.

The fault was interrupted by a overcurrent relay. Since the distribution network operates ungrounded with an isolated neutral, the fault can be due to a three-phase or a phase-to-phase short circuit. Fig. 8 can be used to distinguish between these two types of faults. It was observed that this event produced large transients on two phases only which strongly implied a phase-to-phase fault. Note that, for this specific fault type only the differential propagation mode is of interest [15,16]. Therefore, the CWT analysis is applied to a transient obtained as the difference between the voltage signals of the two faulted phases (A and B).

Since the tower geometry of the overhead lines in this distribution network are the same as shown in [11], the differential propagation speed is determined as $2.94 \cdot 10^8$ m/s for the identification of the characteristic frequencies defined in (1).

The characteristic frequency associated with the fault location is calculated as the interval of frequencies corresponding to the paths between the observation point, Node 01, and Nodes 07 and 08 that delimit the faulted line (as shown by Fig. 7). Table III shows the characteristic frequencies calculated by (1).

TABLE III. CHARACTERISTIC AND CWT IDENTIFIED FREQUENCIES USING THE APPROACH OF [11,12] RELEVANT TO THE PROPAGATION PATHS OF TOPOLOGIES REPORTED IN FIG. 7.

Path	Path length $n_p \cdot L_p$ (km)	Theoretical frequencies $f_{p,i}$ (traveling speed equal to $2.94 \cdot 10^8$ m/s) (kHz)	CWT identified frequencies $f_{p,i}$ by using the $E_{cwt}(a)$ (kHz)
Node 01-02	2x2.79 (n_p=2)	52.65	50.25
Node 01-03	4x1.76 (n_p=4)	41.88	38.35
Node 01-04	2x2.34 (n_p=2)	62.81	62.10
Node 01-05	4x2.90 (n_p=4)	25.35	25.95
Node 01-06	2x9.03 (n_p=2)	16.28	18.25
Node 01-07	4x4.79 (n_p=4)	15.35	13.40
Node 01-08	4x6.43 (n_p=4)	11.44	

Fig. 8 shows the obtained scalogram of the signal energy values $E_{cwt}(a)$ provided by (3) by applying the CWT to the fault transient of Fig. 8. The scalogram of Fig. 9 is used to identify the characteristic frequencies also reported in Table III.

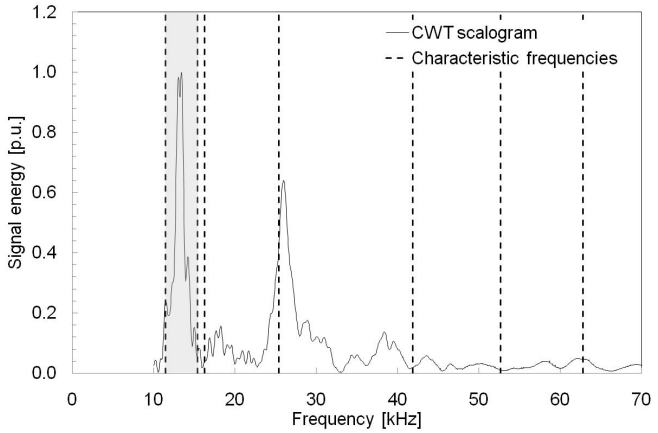

Fig. 9. Energy scalogram relevant to the CWT analysis of a fault transient related to a fault event occurred between Node07 and Node08 of the distribution network of Fig. 7.

As shown by Table III, the identified fault location frequency is equal to 13.4 kHz a value included in the interval between the characteristic frequencies associated to Nodes 07 and 08, namely 11.44 and 15.35 kHz. By applying (1), such an identified frequency corresponds to a distance of 5.485 km from the measurement point Node 01.

Similar to the other cases, Fig. 10 shows the analysis relevant to the identification of time differences between local maximum of the coefficients $C(a,b)$ in the frequency range centered in the CWT identified frequencies $f_{p,i}$ by using the $E_{cwt}(a)$. The results of Fig. 10, allows to identify a time difference of 75.7 μs that corresponds to an identified characteristic frequency of 13.21 kHz. Such a frequency is also in the interval between the characteristic frequencies associated to Nodes 07 and 08, namely 11.44 and 15.35 kHz.

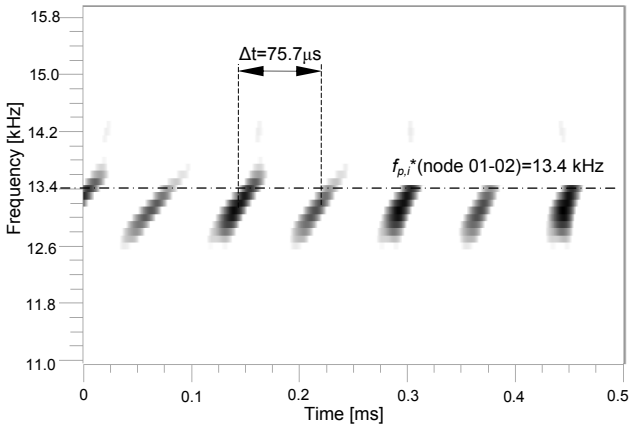

Fig. 10. Coefficients $C(a,b)$ obtained by means of the CWT analysis applied to the fault transient of Fig. 8: improved estimation of the characteristic frequency associated to the faulted path between Nodes 01-07 and 01-08.

V. CONCLUSIONS

This paper describes a fault location procedure based on the CWT analysis of fault-originated transients. Compared to the previously developed procedure, it integrates both time and frequency information obtained from the CWT decompositions. The proposed procedure consists of two-steps: (1) initial estimation of the characteristic frequencies associated with the fault location by using the approach proposed in [11,12]; (2) improvement of the estimate by identifying the time differences between local maximum of the signal coefficients $C(a,b)$ defined by the CWT (2) in the frequency range centered at the previously identified frequencies.

The procedure is successfully applied to fault transient waveforms which are obtained experimentally during various fault scenarios, specially staged in reduced scale setup of a cable distribution network feeder. Test results confirm the superiority of the proposed procedure compared to the one presented in [11,12] in terms of overall accuracy of the fault location.

Finally, the availability of a fault transient recorded in a real distribution network with known characteristics, allowed validation of the proposed procedure when applied to an actual distribution system.

ACKNOWLEDGMENT

The authors would like to thank Prof. C.A. Nucci for the useful discussions and comments during the preparation of this manuscript.

REFERENCES

[1] CIRED WG03 Fault management, "Fault management in electrical distribution systems", 1998.

[2] IEEE Std C37.114, "IEEE guide for determining fault location on AC transmission and distribution lines", 2004.

[3] M. S. Sachdev and R. Agarwal, "A technique for estimating transmission line fault locations from digital impedance relay measurements" IEEE Trans. on PWRD, vol. 3, no. 1, pp. 121–129, Jan. 1988.

[4] K. Srinivasan and A. St.-Jacques, “A new fault location algorithm for radial transmission lines with loads,” IEEE Trans. on PWRD, vol. 4, no. 3, pp. 1676–1682, Jul. 1989.
[5] A. A. Girgis, D. G. Hart, and W. L. Peterson, “A new fault location technique for two- and three-terminal lines,” IEEE Trans. on PWRD, vol. 7, no. 1, pp. 98–107, Jan. 1992.
[6] G. B. Ancell and N. C. Pahalawatha, “Maximum likelihood estimation of fault location on transmission lines using travelling waves,” IEEE Trans. on PWRD, vol. 9, no. 2, pp. 680–689, Apr. 1994.
[7] O. Chaari, M. Meunier, and F. Brouaye, “Wavelets: A new tool for resonant grounded power distribution systems relaying,” IEEE Trans. on PWRD, vol. 11, no. 3, pp. 1301–1308, Jul. 1996.
[8] F. H. Magnago and A. Abur, “Fault location using wavelets,” IEEE Trans. on PWRD, vol. 13, no. 4, pp. 1475–1480, Oct. 1998.
[9] F. H. Magnago and A. Abur, “A new fault location technique for radial distribution systems based on high frequency signals,” in Proc. IEEE-Power Eng. Soc. Summer Meeting, vol. 1, pp. 426–431, Jul. 18–22, 1999.
[10] D. W. P. Thomas, R. E. Batty, C. Christopoulos, and A. Wang, “A novel transmission-line voltage measuring method,” IEEE Trans. Instrum. Meas., vol. 47, no. 5, pp. 1265–1270, Oct. 1998.
[11] A. Borghetti, S. Corsi, C. A. Nucci, M. Paolone, L. Peretto, and R. Tinarelli, “On the use of continuous-wavelet transform for fault location in distribution power networks,” Elect. Power Energy Syst., vol. 28, pp. 608–617, 2006.
[12] A. Borghetti, M. Bosetti, M. Di Silvestro, C.A. Nucci and M. Paolone, “Continuous-Wavelet Transform for Fault Location in Distribution Power Networks: Definition of Mother Wavelets Inferred from Fault Originated Transients”, IEEE Trans. on PWRS, vol. 23, no. 2, pp.380-388, may 2008.
[13] M. Kezunovic, M. Aganagic, V. Skendzic, J. Domaszewicz, J.K. Bladow, D.M. Hamai, S.M. McKenna, “Transients computation for relay testing in real-time”, IEEE Trans. on PWRD, vol. 9, no. 3, pp.1298 – 1307, July 1994.
[14] H.Y. Li, Z.Q. Bo, B. Caunce, S. Potts, “A fault transient comparison technique for multi-ended distribution feeders”, 7th Int. Conf. on Developments in Power System Protection (IEE), 9-12 April 2001 pp.153 – 156
[15] E. Clarke, Circuit analysis of AC power systems, 1. New York: John Wiley & Sons; 1943.
[16] H.W. Dommel, “Digital computer solution of electromagnetic transients in single and multi-phase networks”, IEEE Trans. on PAS, vol. 88, pp. 388-99, April 1969.
[17] A. Graps, “An introduction to wavelets,” IEEE Comput. Sci. Eng., vol. 2, no. 2, pp. 50–61, Summer, 1995.
[18] T. Lobos, T. Sikorski, P. Schegner, “Joint time-frequency representation of non-stationary signals in electrical power engineering”, Proc. of the 15th Power Systems Computation Conference (PSCC'05), Liege, Belgium, 22-26 August 2005, paper fp 97.
[19] K. Yamabuki, A. Borghetti, F. Napolitano, C.A. Nucci, M. Paolone, L. Peretto, R. Tinarelli, M. Bernardi, R. Vitale, “A Distributed Measurement System for Correlating Faults to Lightning in Distribution Networks”, Proc of the International Symposium on High Voltage Engineering, Ljubljana, Slovenia, 27-31 Aug. 2007.
[20] A. Borghetti, F. Napolitano, C.A. Nucci, M. Paolone, M. Bernardi, F. Rachidi, K. Yamabuki, “Correlation of lightning events and faults in distribution power networks: a joint research project”, Proc. of the Cigre Session 2008, August, 24 - 29 2008, Paris, France, paper C4-117.
[21] M. Bernardi, C. Giorgi, V. Biscaglia, “Medium voltage line faults correlation with lightning events recorded with the Italian LLP system CESI-SIRF”, Proc. 24th International Conference on Lightning Protection, Birmingham-UK, 1998, vol.1, pp. 187-192.